metals

MDPI

Article

Hydrogen Generation from Mg Wastes by Cold Rolling and Ball Milling by Hydrolysis Reaction: Elektron 21 (UNS-M12310) in Simulated Seawater

Guillaume Donadey, Simon Caillaud, Pierre Coeuret, Maria Moussa, Laurent Cuzacq and Jean-Louis Bobet *

ICMCB, CNRS, Université de Bordeaux, UMR 5026, F-33600 Pessac, France
* Correspondence: jean-louis.bobet@u-bordeaux.fr

Abstract: Hydrolysis is an efficient way of producing hydrogen by using Mg-based waste. In this study, H_2 production is realized in simulated seawater (i.e., 3.5 wt.% NaCl) using the Elektron21 (EL21) alloy as a reagent. This alloy is a magnesium-based alloy composed of 96 wt.% Mg and 4 wt.% rare earth (approx. 3 wt.% Nd and 1 wt.% Gd). EL21 is known for its excellent corrosion resistance and high tensile strength. The impact of different mechanical treatments (ball milling, cold rolling, cryo rolling, and cryo ball milling) on the hydrolysis yield of the material was discussed. A pretreatment with cryo rolling before ball-milling treatment shows the best hydrolysis performance, with a yield of 90.5% achieved in 10 min in salted water. The ductile-to-brittle transition induced a modification of the microstructure, which explains the good hydrolysis performances.

Keywords: green hydrogen; hydrolysis; magnesium alloys

check for updates

Citation: Donadey, G.; Caillaud, S.; Coeuret, P.; Moussa, M.; Cuzacq, L.; Bobet, J.-L. Hydrogen Generation from Mg Wastes by Cold Rolling and Ball Milling by Hydrolysis Reaction: Elektron 21 (UNS-M12310) in Simulated Seawater. *Metals* **2022**, *12*, 1821. https://doi.org/10.3390/met12111821

Academic Editor: Tomasz Czujko

Received: 11 October 2022
Accepted: 24 October 2022
Published: 27 October 2022

Publisher's Note: MDPI stays neutral with regard to jurisdictional claims in published maps and institutional affiliations.

Copyright: © 2022 by the authors. Licensee MDPI, Basel, Switzerland. This article is an open access article distributed under the terms and conditions of the Creative Commons Attribution (CC BY) license (https://creativecommons.org/licenses/by/4.0/).

1. Introduction

Thanks to its high energy density per mass, cleanness, and abundance, hydrogen is one of the best energy carriers [1]. By using it in a fuel cell or by burning it directly, hydrogen can contribute to greenhouse gas reduction (no emission of CO_2, only H_2O). Therefore, hydrogen can also be used as a means of locomotion or to produce electricity.

However, in addition to the cost, hydrogen storage [2] and production [3] are still the factors limiting the commercial application of this element. Currently, the most used method to produce hydrogen is through the use of fossil fuels (by different methods: catalytic steam reforming, coal gasification, and partial oxidation) for almost 95% [4] or electrolysis for 5% [5]. By using cleaner and/or easier methods of producing hydrogen, it may be possible to increase the range of possible applications. For instance, in order to produce hydrogen on demand, the hydrolysis of magnesium waste seems to be a good solution in order to give the waste a second life [6–14]. In fact, magnesium and its alloys have a low density (thus a high hydrolysis yield), low cost, and low toxicity, as well as being abundant. Moreover, on-demand production would solve the problem of the storage and distribution of hydrogen. It will be a three-in-one solution to Mg waste valorization (as the end product, $Mg(OH)_2$ will be non-hazardous).

Elektron 21 (UNS-M12310) is a light and durable alloy that is used in different fields: aerospace, military, or motorsport applications. This alloy is composed of magnesium (96 wt.%), neodymium (2.6–3.1 wt.%), and gadolinium (1–1.7 wt.%) [15]. The machining of these alloys produces waste in the form of chips. Currently, this produced waste is not valorized since recycling is prohibitively expensive.

The goal of this study is to find a good way to reuse these metal scraps coming from industrial waste and give them a second life as a hydrogen generator. This goal can be achieved by reacting this alloy with water thanks to the reaction:

$$Mg\ (s) + 2H_2O\ (l) \rightarrow Mg(OH)_2\ (s) + H_2\ (g)\ \Delta Hr = -354\ kJ{\cdot}mol^{-1} \quad (1)$$

Some studies have already shown that the production of hydrogen from ball milling magnesium and using different additives [6,12,16–22] and different reactive solutions [13,23,24] increases the yield of the reaction.

The hydrolysis reaction is a great way to produce hydrogen: it only needs water, and there is no need for extra energy to start the reaction (low-temperature operation). In addition, this method offers rather pure hydrogen (some water vapor can be present, but as PEMFC requires water vapor for optimum operation, it is an advantage).

The biggest issue with this method for the hydrolysis of magnesium is the formation of a passivation layer of $Mg(OH)_2$ on the surface of the alloy, which prevents contact between water and unreacted Mg, thus limiting hydrolysis [16].

By performing the reaction in salted water (i.e., simulated seawater) [25], the passivation layer is broken by the formation of $MgCl_2$, which has a higher solubility than $Mg(OH)_2$ This formation of soluble $MgCl_2$ creates channels where the water penetrates to reach the core of Mg. The presence of Cl^- in the water prevents the agglomeration of $Mg(OH)_2$ particles around unreacted Mg. The main objective of this study is to apply various mechanical treatments to EL21 alloy, to improve the hydrolysis reaction. All the results will be discussed in regard to the XRD analysis (cell parameters and crystallite size) and the SEM and granulometry measurement (morphology and specific surface). Modeling will be performed to better understand the reactive mechanism.

2. Experimental Details

All the cold-rolling (CR) treatments were performed by laying magnesium alloy scraps between two sheets of stainless steel and then rolling the sheets. The different parameters modified are the number of passes through the rolling setup. For cryogenic rolling (CryoR), the stainless plates were immersed inside liquid nitrogen for 10 min, then the sample was placed between the plates and rolled.

Ball milling (BM) of the magnesium alloy (using a Fritsch-Pulverisette 5, FRITSCH GmbH, Idar-Oberstein, Germany) was performed under argon at a rotation speed of 250 rpm/min for 1 h (four cycles of 15 min of milling then 2 min of rest). The ball to powder weight ratio is 17:1, corresponding to 8 g of powder and 34 balls (10 mm in diameter). For cryogenic ball milling (cryoBM), the setup was immersed in liquid nitrogen for 10 min. It was then used in the milling machine for 15 min. This operation was repeated four times (e.g., replacing the rest of the 2 min).

Hydrolysis tests were carried out between 25 °C and 37 °C in a simulated seawater solution (3.5% NaCl) using a homemade experimental setup [26]. In order to reach the full reaction (i.e., obtain the total yield), 1 mL of hydrochloric acid was added to the water at the end of the reaction (after 1 h usually).

The samples were characterized by X-ray diffraction (XRD) using a PANalytical X'Pert (PW1820, Malvern Pan Analytical, Palaiseau, France) diffractometer with Cu kα_1 radiation (λ = 15,405 Å). Crystallite sizes (according to the weighted Scherrer formula) and cell parameters were estimated from XRD using EVA software.

Scanning electron microscope observations were made using a Tescan Vega3 SB microscope (TESCAN ORSAY HOLDING, a.s. Brno – Kohoutovice, Czech Republic) equipped with a secondary electron (SE) detector, a backscattered electron detector (BSE), and an energy dispersive X-ray spectrometer (EDS) for the elemental surface composition analysis.

3. Results and Discussion

The XRD analysis of all the samples, presented in Figure 1, shows the presence of magnesium peaks only (PDF 01-089-4894). For the ball-milled sample, the aluminum peaks come from the sample holder.

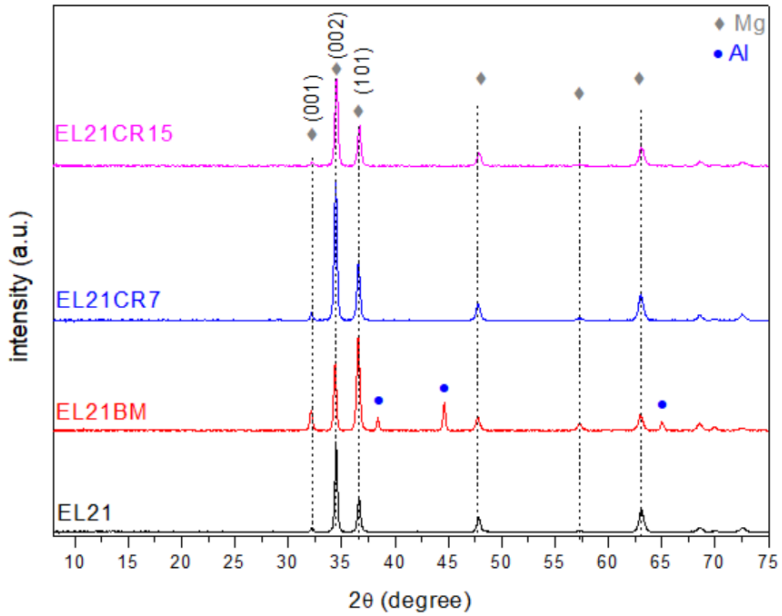


Figure 1. X-ray diffraction patterns of EL21, EL21 ball milled, EL21 cold rolled 7 times, and EL21 cold rolled 15 times.

EL21, in contrast to pure magnesium, has a preferential orientation along the c-axis, as shown by the relative intensity of the peaks at 34.4° (Plane 002) and 35.5° (Plane 101) (maximum intensity for Plane 002). The cold-rolled samples do not change this preferential orientation of the alloy since low deformation energy is involved. However, with higher energy (i.e., ball milling), the preferential orientation disappears. By analyzing the XRD pattern (Table 1), we can see that the lattice parameters for all samples are approximately the same and close to those of pure magnesium.

Table 1. Cell parameters and crystallite size of pure magnesium and the different alloys before and after treatment.

	EL21	**EL21-BM**	**EL21-CR7**	**EL21-CR15**	**Mg (According to ICSD n° 01-089-4894)**
a (Å)	3.212 (3)	3.218 (4)	3.214 (4)	3.213 (4)	3.209
c (Å)	5.203 (5)	5.216 (7)	5.208 (7)	5.197 (7)	5.210
L_{002} (nm)	36 (2)	34 (3)	30 (3)	28 (3)	
L_{101} (nm)	32 (2)	30 (3)	34 (3)	32 (3)	

EL21 contains 4 wt.% rare earth. As the metallic radius of RE is larger than that of Mg (1.82 nm and 1.80 nm for Nd and Gd, respectively [27] vs. 1.60 nm for Mg), a slight increase in the cell parameter can be expected (in the case of a solid solution). Therefore, 4 wt.% represents only 0.65 mol%, and so the variation would be very limited.

Along the c-axis (L_{002}), the crystallite size seems to decrease when the number of cold-rolling passes increases. For the ball-milled sample, a small decrease in the crystallite size in both directions is noticed. By comparing the values of the crystallite size between EL21 and EL21CR15, we can see that along the c-axis, the crystallite size decreases, but along both the a- and c-axes (Plane 101), the crystallite size does not change, meaning that along the a-axis, the crystallite size increases. It is then possible to conclude that the variation of the crystallite size is anisotropic.

For all the cold-rolling treatments, the surface of the alloy was flattened. We also do not observe a significant change in thickness between CR3, CR7, and CR15.

Thanks to the SEM observation (Figure 2), we were able to highlight that CR3 does not exhibit a lot of small cracks (surface defects). For CR7, some big cracks are present but

also some small ones. Increasing the cold-rolling passes (from three to seven) leads to the presence of numerous defects. However, comparing the CR15 sample with CR7, we can notice that some of the small cracks (present on the CR7 sample) are welded back together, so the number of cracks seems to decrease a little.

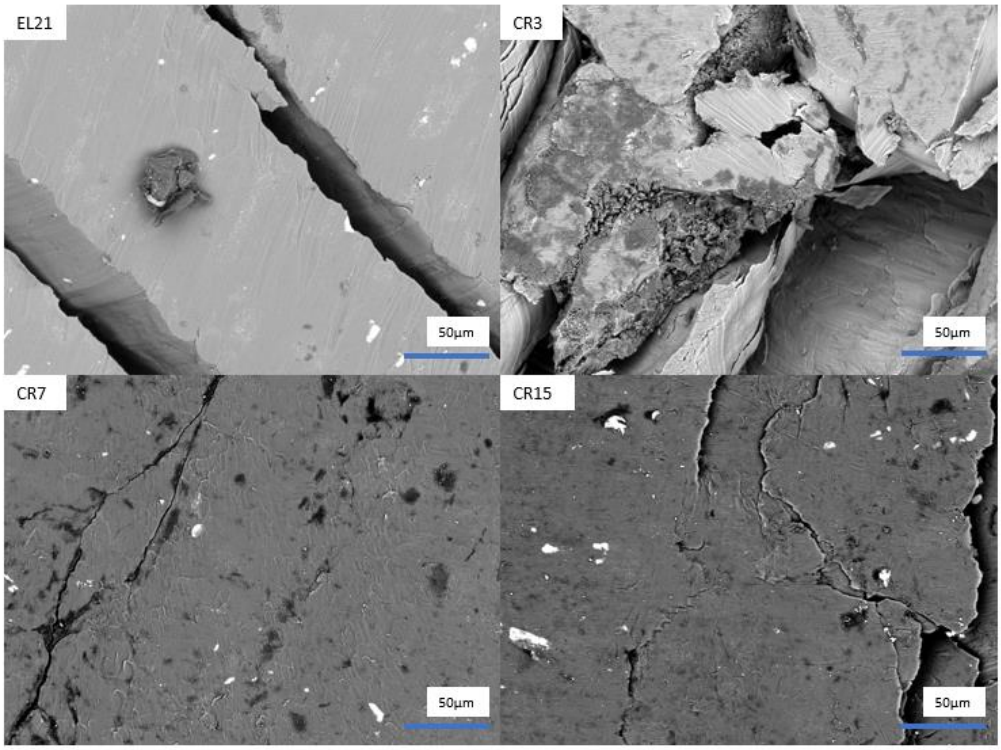


Figure 2. SEM images of EL21 after different mechanical treatment.

Hydrogen generation for some samples is reported in Figure 3. The hydrolysis of the as-received EL21 is very slow and weak (5% yield after 2 h) (Figure 3). The EL21 sample without mechanical treatment is a material that has a specific surface and is known to resist corrosion, so it is normal that it does not react a lot with water.

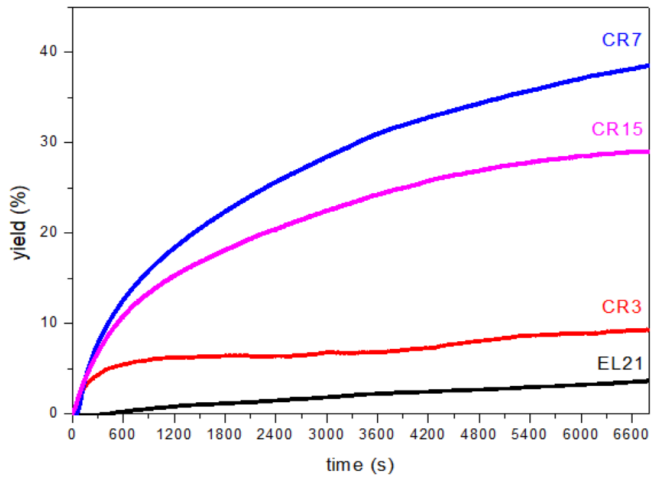


Figure 3. Hydrogen generation kinetics and yield of EL21 after different mechanical treatment in salted water.

Cold rolling increases the hydrolysis yield, with an optimum between CR3 and CR15 for CR7. Nevertheless, cold rolling seven times after 1 h only produces 28.5% hydrogen. By comparison, Huang et al. [19] obtained after 1 h in seawater a yield of 27.5% with pure magnesium powder.

Since the yield of CR15 is lower than that of CR7, we can deduce that a too-severe mechanical treatment can negatively impact the hydrogen generation of the material. Then, it is possible to conclude that the number of cracks (cf. previous paragraph, Figure 2) impacts the specific contact surface between Mg and H_2O, thus increasing the efficiency of the hydrolysis.

Nevertheless, the maximum yield remains low, and, so, in order to have a better hydrolysis yield, another mechanical treatment might be necessary. Ball milling, cryogenic rolling, and cryogenic ball milling were tested for that purpose.

Ball milling is influenced by a lot of different parameters such as the type of miller, ball to powder weight ratio, milling speed, milling time, milling atmosphere, etc. As the ball-milling process generates a lot of heat and can therefore lead to the agglomeration of particles, a rest period is necessary to help the sample to cool down. That is why in our process, ball milling was performed for 15′, and a rest of 2′ was applied.

According to that, this process helps to reduce the size of the particles. This reduction in size helps to increase the specific surface contact area of the particles and thus increases the kinetics and hydrolysis yield of the samples.

In addition, as explained by Bacha et al. [13], increasing the milling time without additives beyond 2 h reduces the hydrolysis performance. Grosjean et al. [24] were the first to report the beneficial effect of milling on the increase in corrosion of Mg and therefore on its hydrolysis. It has also been described that milling under argon leads to better results than milling under H_2 [20].

SEM observations of the sample cryo rolled seven times with subsequent ball milling are presented in Figure 4. Comparing Figures 2 and 4 for CR7 and cryoCR7 clearly highlights that the number of cracks/defects is comparable in both cases. This means that the temperature is not low enough to have the ductile–brittle transition for the magnesium alloy. Ball milling (Figure 4) leads to a huge decrease in particle size. The sample is in the form of a rough powder.

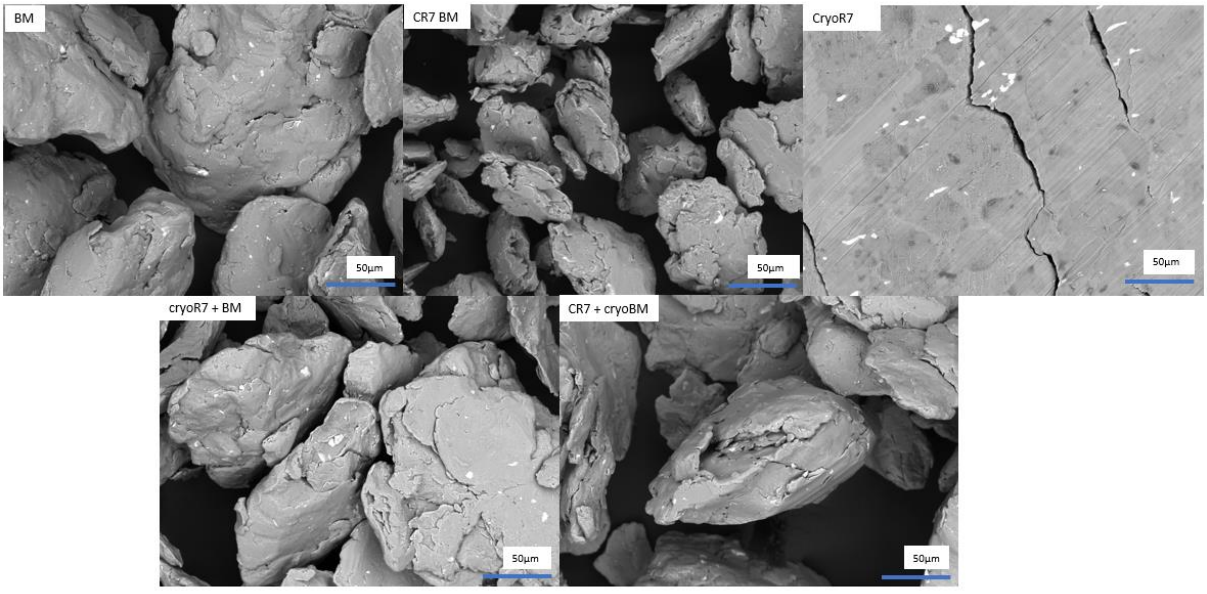


Figure 4. SEM micrograph of the sample cryo rolled 7 times and the ball-milled samples with different mechanical treatments.

We can see on the SEM micrographs that the particle sizes are different after ball milling.

For the BM sample, the particle sizes are larger than 100 µm; for the cryoR7+BM and CR7+CryoBM samples, they are around 100 µm, and for the CR7+BM sample, the particles have a size inferior to 100 µm. For these cold-rolled samples and cryo-rolled ball-milled samples, they all have a platelet shape thanks to the mechanical treatment performed before the milling. Only the ball-milled samples have a more spherical and

smoother shape (without a lot of surface defects) in comparison with the other samples. By comparing the ball-milled sample with the cold-rolled then ball-milled sample, we can see that the treatment with CR7 considerably reduces the particle size, thus increasing the surface contact of these particles with water (thus higher yield). We also do not observe a lot of differences between the particle size and shape of the cryoR7+BM samples and the CR7+cryoBM sample.

By performing SEM/EDS analysis, we were able to see three different types of phases. The one that appears white corresponds to rare earth (e.g., gadolinium and neodymium). The gray phase (the major phase) was composed of almost pure magnesium with a very low amount of rare earth (within the detection limit of the EDS analysis). Additionally, some traces of MgO were also detected.

The hydrolysis performances of these mechanically treated materials were measured and are reported in Figure 5. From this figure, we observe that the sample cryo rolled seven times has a hydrolysis performance below that just cold rolled seven times.

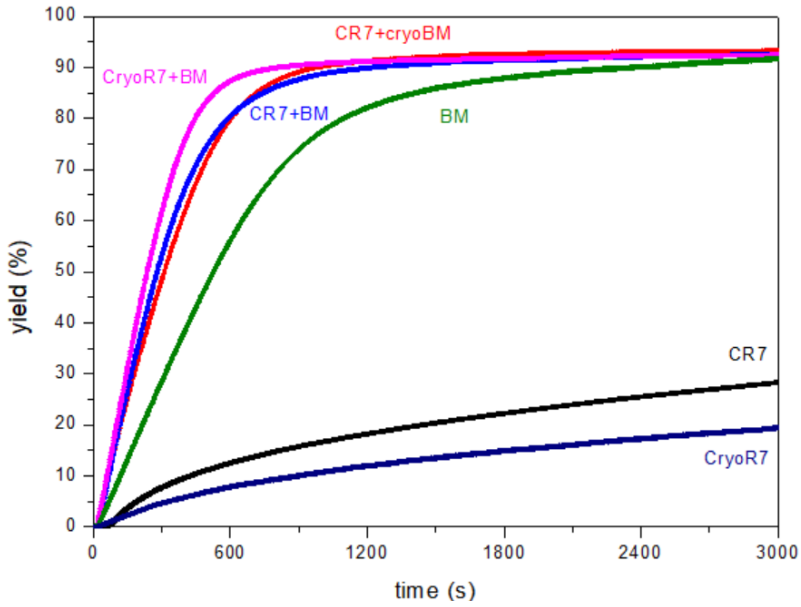


Figure 5. Hydrogen generation kinetics and yield of EL21 after cold rolling and/or ball milling.

As observed, by cold rolling the samples before BM, we can obtain higher kinetics than without CR (Figure 5). This could be explained by the absence (or very limited number) of cracks on the surface of the sample (see Figure 4). The reduced number of cracks decreases the reactive surface area between Mg and H_2O. It is noticed that after 10 min, all the BM samples have completely reacted (Figure 5).

By changing the treatment from ball milling to cryo ball milling, we do not notice any significant change in the hydrolysis kinetics or yield. For all the ball-milling treatments, we observe a plateau at around 90.5%. This could happen because the samples are a bit old, and there could be oxidation of a part of the Mg that prevents the formation of $MgO/Mg(OH)_2$ and thus H_2. The darker gray phase found on the SEM/EDS sample (attributed to MgO) could explain the plateau at 90.5%.

In order to obtain a deeper understanding of the hydrolysis behavior, various models were tried. It is possible to see in Figure 6 that the Avrami model fits the hydrolysis yield for this sample really well, which is also the case for all the other samples.

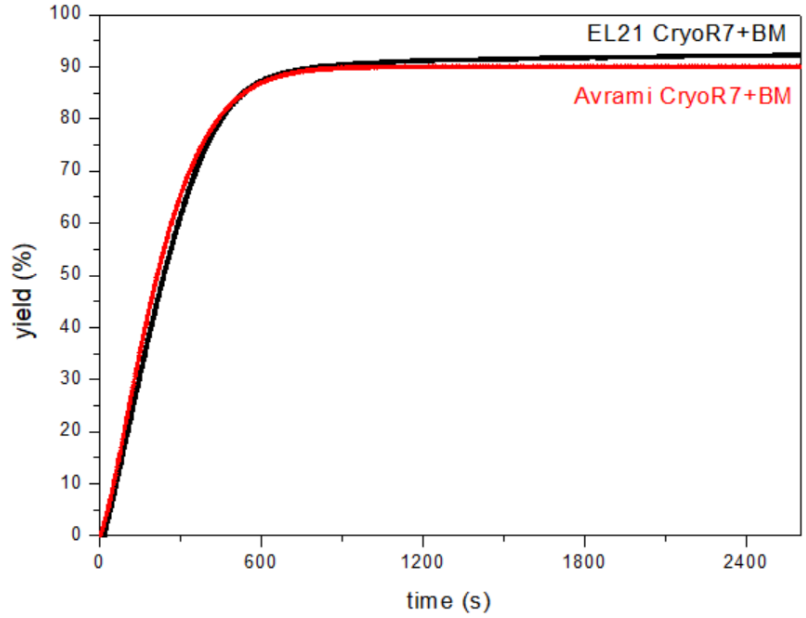


Figure 6. Hydrogen generation kinetics and yield of EL21 CryoR7+BM and the Avrami model of the same sample.

By comparing the different orders of reaction n reported in Table 2, it is shown that the order of reaction for all the ball-milled samples stays between 1 and 2, and that the cold-rolled samples are around 1 or below this value. We can maybe understand that there is a change in the type of controlled reaction.

Table 2. Order of reaction and kinetic constant of the different samples by using the Avrami model.

	CryoR7BM	CR7+CryoBM	CR7+bm	BM	CR7	CryoR7
n	1.381	1.276	1.278	1.328	0.958	0.882
k (T^{-1})	4.9×10^{-4}	6.0×10^{-4}	6.5×10^{-4}	2.0×10^{-4}	1.2×10^{-3}	1.2×10^{-3}

As explained by Sharp et al. [28,29], the ball-milled particles are more susceptible to react as a phase-boundary-controlled reaction (R_3) (reaction is controlled by the movement of the interface at a constant velocity; it reacts from the surface inward), and the cold-rolled and cryo-rolled samples are more susceptible to follow a first-order kinetics reaction (F_1) (random germination then instantaneous growth).

The various equations to be used are then:

$f(t) = 1 - e^{-kt^n}$ For the Avrami model

$F_1(\alpha) = Ln(1-\alpha) = -kt$ with α the fraction of total product to the time of reaction t

$R_3(\alpha) = \left(1 - (1-\alpha)^{\frac{1}{3}}\right) = \left(\frac{u}{r}t\right)$ with r the radius of the particle and u the movement of the interface at a constant velocity

For the kinetic part, the variation of the kinetic constant (Table 2) is very limited between the different treatments, but a larger kinetic constant for the slowest reactions is reported. This difference between the model and the reality may come from the difference in the activation energy (AE) between all the samples. For the cold-rolled samples, the AE may be high, which is why there is a decrease in the overall kinetics of the reactions. The AE was not determined since in an aqueous environment, the difference in temperature is around 50° (under 10 °C the kinetics are too slow, and over 60 °C, there is the formation of vapor), which provides a high inaccuracy of the measurement of the activation energy.

4. Conclusions

In conclusion, we investigated the different strategies for hydrogen production from the alloy Elektron21. Ball milling allows suppressing the preferential orientation of the alloys along the c-axis.

Cryo rolling tends to change the properties from ductile to brittle behavior, and thanks to that, increases, after ball milling, the hydrolysis kinetics by increasing the surface of the sample reacting with water. Nevertheless, the temperature is not low enough to have a full ductile to brittle transition, so the effect is limited.

It has been shown that ball milling under argon is one of the best ways to have high kinetics of hydrolysis, but cold rolling before ball milling helps the kinetics even further for H_2 production. After 1 h of hydrolysis, CR7 has a hydrogen yield of 28.5%, and for CR7+BM, the hydrogen yield increases to 90%.

Author Contributions: Conceptualization, S.C., P.C., M.M., L.C. and G.D.; methodology, S.C., P.C., M.M., L.C. and G.D.; validation, J.-L.B.; formal analysis, J.-L.B.; investigation, S.C., P.C., M.M., L.C. and G.D.; writing—original draft preparation, G.D.; writing—review and editing, J.-L.B.; supervision, J.-L.B.; project administration, J.-L.B. All authors have read and agreed to the published version of the manuscript.

Funding: This research received no external funding.

Data Availability Statement: Available upon request.

Conflicts of Interest: The authors declare no conflict of interest.

References

1. Oshiro, K.; Fujimori, S. Role of hydrogen-based energy carriers as an alternative option to reduce residual emissions associated with mid-century decarbonization goals. *Appl. Energy* **2022**, *313*, 118803. [CrossRef]
2. Usman, M.R. Hydrogen storage methods: Review and current status. *Renew. Sustain. Energy Rev.* **2022**, *167*, 112743. [CrossRef]
3. Younas, M.; Shafique, S.; Hafeez, A.; Javed, F.; Rehman, F. An Overview of Hydrogen Production: Current Status, Potential, and Challenges. *Fuel* **2022**, *316*, 123317. [CrossRef]
4. Dicks, A.L. Hydrogen generation from natural gas for the fuel cell systems of tomorrow. *J. Power Sources* **1996**, *61*, 113–124. [CrossRef]
5. Bhandari, R.; Trudewind, C.A.; Zapp, P. Life cycle assessment of hydrogen production via electrolysis—A review. *J. Clean. Prod.* **2014**, *85*, 151–163. [CrossRef]
6. Oh, S.K.; Cho, T.; Kim, M.; Lim, J.; Eom, K.; Kim, D.; Cho, E.; Kwon, H. Fabrication of Mg–Ni–Sn alloys for fast hydrogen generation in seawater. *Int. J. Hydrogen Energy* **2017**, *42*, 7761–7769. [CrossRef]
7. Uan, J.-Y.; Cho, C.-Y.; Liu, K.-T. Generation of hydrogen from magnesium alloy scraps catalyzed by platinum-coated titanium net in NaCl aqueous solution. *Int. J. Hydrogen Energy* **2007**, *32*, 2337–2343. [CrossRef]
8. Uan, J.-Y.; Yu, S.-H.; Lin, M.-C.; Chen, L.-F.; Lin, H.-I. Evolution of hydrogen from magnesium alloy scraps in citric acid-added seawater without catalyst. *Int. J. Hydrogen Energy* **2009**, *34*, 6137–6142. [CrossRef]
9. AlBacha, S.; Thienpont, A.; Zakhour, M.; Nakhl, M.; Bobet, J.L. Clean hydrogen production by the hydrolysis of magnesium-based material: Effect of the hydrolysis solution. *J. Clean. Prod.* **2021**, *282*, 124498–124507. [CrossRef]
10. Figen, A.K.; Coşkuner, B.; Pişkin, S. Hydrogen generation from waste Mg based material in various saline solutions ($NiCl_2$, $CoCl_2$, $CuCl_2$, $FeCl_3$, $MnCl_2$). *Int. J. Hydrogen Energy* **2015**, *40*, 7483–7489. [CrossRef]
11. Rodríguez, M.; Niro, F.; Urretavizcaya, G.; Bobet, J.-L.; Castro, F.J. Hydrogen production from hydrolysis of magnesium wastes reprocessed by mechanical milling under air. *Int. J. Hydrogen Energy* **2022**, *47*, 5074–5084. [CrossRef]
12. Bai, J.; Li, D.; Cao, Q.; Hou, X.; Xu, Y. Hydrolysis H2 generation behavior of AM50 alloy waste coactivated by Mg-based master alloys. *Int. J. Hydrogen Energy* **2022**, *47*, 31191–31201. [CrossRef]
13. Al Bacha, S.; Pighin, S.; Urretavizcaya, G.; Zakhour, M.; Nakhl, M.; Castro, F.; Bobet, J.-L. Effect of ball milling strategy (milling device for scaling-up) on the hydrolysis performance of Mg alloy waste. *Int. J. Hydrogen Energy* **2020**, *45*, 20883–20893. [CrossRef]
14. Figen, A.K.; Filiz, B.C. Hydrogen production by the hydrolysis of milled waste magnesium scraps in nickel chloride solutions and nickel chloride added in Marmara Sea and Aegean Sea Water. *Int. J. Hydrogen Energy* **2015**, *40*, 16169–16177. [CrossRef]
15. Mouls, B.; Arurault, L.; Taberna, P.-L.; Bonningue, C. Macroscopic, thermodynamic, kinetic and microscopic study of nitric acid pickling of Elektron 21 (EV31A) magnesium alloy. *J. Magnes. Alloys* **2014**, *2*, 363–376. [CrossRef]
16. Awad, A.S.; El-Asmar, E.; Tayeh, T.; Mauvy, F.; Nakhl, M.; Zakhour, M.; Bobet, J.-L. Effect of carbons (G and CFs), TM (Ni, Fe and Al) and oxides (Nb_2O_5 and V_2O_5) on hydrogen generation from ball milled Mg-based hydrolysis reaction for fuel cell. *Energy* **2016**, *95*, 175–186. [CrossRef]

17. Grosjean, M.-H.; Roué, L. Hydrolysis of Mg–salt and MgH_2–salt mixtures prepared by ball milling for hydrogen production. *J. Alloys Compd.* **2006**, *416*, 296–302. [CrossRef]
18. Wang, S.; Sun, L.-X.; Xu, F.; Jiao, C.-L.; Zhang, J.; Zhou, H.-Y.; Huang, F.-L. Hydrolysis reaction of ball-milled Mg-metal chlorides composite for hydrogen generation for fuel cells. *Int. J. Hydrogen Energy* **2012**, *37*, 6771–6775. [CrossRef]
19. Huang, M.; Ouyang, L.; Chen, Z.; Peng, C.; Zhu, X.; Zhu, M. Hydrogen production via hydrolysis of Mg-oxide composites. *Int. J. Hydrogen Energy* **2017**, *42*, 22305–22311. [CrossRef]
20. Tayeh, T.; Awad, A.S.; Nakhl, M.; Zakhour, M.; Silvain, J.-F.; Bobet, J.-L. Production of hydrogen from magnesium hydrides hydrolysis. *Int. J. Hydrogen Energy* **2014**, *39*, 3109–3117. [CrossRef]
21. Liu, Y.; Wang, X.; Liu, H.; Dong, Z.; Cao, G.; Yan, M. Hydrogen generation from Mg–LiBH4 hydrolysis improved by AlCl3 addition. *Energy* **2014**, *68*, 548–554. [CrossRef]
22. Liu, Y.; Wang, X.; Dong, Z.; Liu, H.; Li, S.; Ge, H.; Yan, M. Hydrogen generation from the hydrolysis of Mg powder ball-milled with AlCl3. *Energy* **2013**, *53*, 147–152. [CrossRef]
23. Shetty, T.; Szpunar, J.A.; Faye, O.; Eduok, U. A comparative study of hydrogen generation by reaction of ball milled mixture of magnesium powder with two water-soluble salts (NaCl and KCl) in hot water. *Int. J. Hydrogen Energy* **2020**, *45*, 25890–25899. [CrossRef]
24. Grosjean, M.-H.; Zidoune, M.; Roué, L.; Huot, J.; Schulz, R. Effect of ball milling on the corrosion resistance of magnesium in aqueous media. *Electrochim. Acta* **2004**, *49*, 2461–2470. [CrossRef]
25. Yu, S.-H.; Uan, J.-Y.; Hsu, T.-L. Effects of concentrations of NaCl and organic acid on generation of hydrogen from magnesium metal scrap. *Int. J. Hydrogen Energy* **2012**, *37*, 3033–3040. [CrossRef]
26. Pighin, S.A.; Urretavizcaya, G.; Bobet, J.-L.; Castro, F.J. Nanostructured Mg for hydrogen production by hydrolysis obtained by MgH2 milling and dehydriding. *J. Alloys Compd.* **2020**, *827*, 154000. [CrossRef]
27. Teatum, E.T., Jr.; Gschneidner, K.A.; Waber, J.T. *Compilation of Calculated Data Useful in Predicting Metallurgical Behavior of the Elements in Binary Alloy Systems*; Los Alamos Scientific Laboratory: Los Alamos, NM, USA, 1968. [CrossRef]
28. Hancock, J.D.; Sharp, J.H. Method of Comparing Solid-State Kinetic Data and Its Application to the Decomposition of Kaolinite, Brucite, and $BaCO_3$. *J. Am. Ceram. Soc.* **1972**, *55*, 74–77. [CrossRef]
29. Sharp, J.H.; Brindley, G.W.; Achar, B.N.N. Numerical Data for Some Commonly Used Solid State Reaction Equations. *J. Am. Ceram. Soc.* **1966**, *49*, 379–382. [CrossRef]